A stable H_2O atmosphere on Europa's trailing hemisphere from HST images

Lorenz Roth

[1]KTH Royal Institute of Technology, Space and Plasma Physics, Teknikringen 31, Stockholm, Sweden

Key Points:

- Eclipse observations limit the abundance of O in Europa's atmosphere to a low level.
- The OI1356-Å/OI1304-Å ratio is lower in the central part of the trailing hemisphere than elsewhere on Europa.
- Modeling of the emissions suggest H_2O to be more abundant than O_2 in the trailing sub-solar region.

Corresponding author: =name=, `=email address=`

Abstract

Studies of the global intensities of the oxygen emissions at 1356 Å and 1304 Å revealed O_2 in Europa's atmosphere. Here we investigate the relative changes of the two oxygen emissions when Europa emerges from eclipse as well as the radial profiles of the relative emissions across the sunlit disk in Hubble Space Telescope observations taken in 1999, 2012, 2014 and 2015 while the moon was at various orbital positions. The eclipse observation constrains the O column density to 6×10^{12} cm^{-2} or lower. We then find that the OI1356-Å/OI1304-Å ratio systematically decreases towards the disk center on the trailing hemisphere. The observed emission ratio pattern and the persistence of it from 1999 to 2015 imply a stable H_2O abundance in the central sunlit trailing hemisphere with an H_2O/O_2 ratio of 12-22. On the leading hemisphere, the emissions are consistent with a pure O_2 atmosphere everywhere across the moon disk.

Plain Language Summary

Observations by the Hubble Space Telescope in far-ultraviolet light of Jupiter's icy moons were used in the past to detect their oxygen atmospheres. Results of a new analysis of images and spectra of the moon Ganymede have recently shown that the same observations also contain information that water vapor is abundant in the atmosphere in addition to oxygen. We use the same analysis here for Europa and find a water vapor atmosphere as well, but only above the orbital trailing hemisphere of the moon.

1 Introduction

Jupiter's moon Europa possesses a tenuous atmosphere that is thought to be constantly replenished by erosion of its water ice surface (McGrath et al., 2009; Johnson et al., 2009). The main species in the bound atmosphere are expected to be O_2, H_2, and H_2O (Shematovich et al., 2005; Smyth & Marconi, 2006). The first evidence for this atmosphere was provided by a far-ultraviolet (FUV) spectrum of Europa taken by the Hubble Space Telescope, which revealed emissions at 1304 Å and 1356 Å. These emissions were related to atomic oxygen multiplets around these wavelengths, but the persistently brighter disk-averaged OI1356 Å emission intensity (Hall et al., 1995; Hall et al., 1998) is in agreement only with electron impact dissociative excitation on *molecular* oxygen as source. The ratio of the intensities of the FUV oxygen multiplets at 1356 Å and 1304 Å, r_γ(OI) =I(OI1365 Å) / I(OI1304 Å), has become a standard diagnostic to probe for atmospheric composition at Jupiter's moons (Cunningham et al., 2015; Feldman et al., 2000; Hansen et al., 2005; Molyneux et al., 2018) or comets (Feldman et al., 2015; Galand et al., 2020).

Roth et al. (2016) analyzed the absolute and relative intensities of the OI1304 Å and OI1356 Å emissions in a dataset of spectral images taken by HST's Space Telescope Imaging Spectrograph (STIS). They found that in images of the orbital leading hemisphere, the near-surface OI1356 Å/OI1304 Å ratio of $r_\gamma(\mathrm{OI}) = 2.10(\pm 0.07)$ is consistent with a pure O_2 bound atmosphere. On the trailing hemisphere, this near-surface ratio was found to be consistently lower with an average of $r_\gamma(\mathrm{OI}) = 1.63(\pm 0.05)$ (see table 2 of Roth et al. (2016)). The different emission ratios r_γ(OI) were interpreted to be due to differing abundance of atomic oxygen. The higher O abundance on the trailing side ($O/O_2 \sim 0.05$) could be explained by preferential production of atomic oxygen from increased electron impact dissociation of O_2, as the trailing side is also the plasma upstream side and more exposed to the plasma impacts (Pospieszalska & Johnson, 1989; Cassidy et al., 2013).

In regions further above the limb of Europa's disk in the images, r_γ(OI) was found to decrease with distance to Europa (or altitude) compared to the near-surface region.

This was explained with an increasing O/O_2 ratio with altitude (Roth et al., 2016), in accordance with Cassini observations (Hansen et al., 2005) and simulations (Shematovich et al., 2005; Smyth & Marconi, 2006).

The relative FUV oxygen emissions at neighboring moon Ganymede show similar behavior with decreasing r_γ(OI) above the limb and the same hemispheric dichotomy, i.e., a lower ratio (r_γ(OI) $<< 2$) above the trailing hemisphere (Molyneux et al., 2018). Using an HST observation of Ganymede directly before and in eclipse of Jupiter, Roth et al. (2021) recently showed that resonant scattering by atomic oxygen is negligible, setting an upper limit on the global abundance of O in the atmosphere. This upper limit effectively rules out atomic O as explanation for a lower oxygen emission ratio in bright emission regions on Ganymede's disk. Investigating the radial profiles of the ratio r_γ(OI) in STIS images Roth et al. (2021), also found that r_γ(OI) systematically decreases from the region around the limb (r_γ(OI) ~ 2) towards the center of the observed disk on both hemispheres. The found profile is shown to be in agreement with an H_2O-dominated atmosphere around the sub-solar point and a O_2-dominated atmosphere away from the sub-solar point. The concentration of H_2O around the sub-solar point and the hemispheric dichotomy with an 6-fold higher estimated H_2O abundance on the trailing hemisphere is in agreement with the difference in ice sublimation yield, given the difference in albedo and thus surface temperature at Ganymede (Leblanc et al., 2017).

Observational evidence for the presence of gaseous H_2O at Europa was provided indirectly through localized H1216 Å (H Lyman-α) and OI1304 Å FUV emission patches near the south pole (Roth, Saur, Retherford, Strobel, et al., 2014) and through infrared emissions from H_2O (Paganini et al., 2019). In both observations, the signal related to water vapor was only marginally significant and interpreted to originate from an active plume source. The interpretation was based on the localized nature of the atomic emissions, the comparably high derived abundances, and the low detection rate suggesting an intermittent nature (Roth, Saur, Retherford, Strobel, et al., 2014; Paganini et al., 2019). Paganini et al. (2019) also mention that their detection was on the leading hemisphere, while charged particle sputtering and sublimation as potential alternative sources for H_2O are expected to be higher on the darker (and thus warmer) trailing (= plasma upstream) hemisphere where no H_2O emissions were found in the same study.

Here, we use the same approach as recently used by Roth et al. (2021) for Ganymede and study in detail the relative brightness of the two oxygen emissions in order to constrain the H_2O and O abundances relative to O_2 in Europa's global atmosphere. First, we compare consecutive exposures taken in and out of eclipse to constrain the O abundance through its possible resonant scattering contribution. Thereafter, we investigate the emission ratio r_γ(OI) in various observations of Europa and its variation across moon's disk.

2 HST/STIS Observations

We have selected nine sets of images (or 'HST visits') from the HST/STIS datasets presented in Roth et al. (2016) considering primarily the signal-to-noise ratio of the weaker and noisier OI1304 Å emissions. For each visit, we have used only the periods in the exposures when the brightness from the Earth's geocorona along the slit is near or below the level of the statistical noise.

For the eclipse test, we use the visit from 23/24 March 2015 (Visit 17 in table 1 of Roth et al. (2016)), which contains two exposures with low-geocorona exposure time of 1615 sec in eclipse and 1820 sec after egress. This is the only visit that includes an eclipse observations with reasonable signal-to-noise ratio and a consecutive exposure out of eclipse as reference.

From the other visits with Europa at various orbital positions, we selected those with total low-geocorona exposure time of at least 140 minutes. All nine visits analyzed here are summarized in Table 1, where we use the original consecutive visit numbers as in table 1 of Roth et al. (2016).

For the eclipse visit, we separately analyze the exposure in eclipse and the exposure in sunlight. The two exposures are shown in figure 4 of Roth et al. (2016). For the other eight visits, we combined all low-geocorona exposure time obtaining one superposed spectral image. Some of the STIS spectral image data analyzed here are displayed in figure S5 of Roth, Saur, Retherford, Strobel, et al. (2014), figure 3 of Roth, Retherford, et al. (2014) and figures 2 and 3 of Roth et al. (2016). We follow our standard processing pipeline for correcting the detector images for background and surface reflection (absent in the eclipse visit) signals, see Roth, Saur, Retherford, Feldman, and Strobel (2014); Roth, Retherford, et al. (2014); Roth et al. (2016), and include the small processing updates from Roth et al. (2021). We furthermore replace the assumption of a uniform disk brightness with the reflectance model from Oren and Nayar (1994) and a roughness parameter of σ=0.57, which was found to provide good agreement with FUV images of Europa (Sparks et al., 2016; Giono et al., 2020).

Finally, 72x72 pixel images containing the two oxygen emission images centered on the spectral axis at 1303.5 Å and 1356.3 Å are extracted from the spectral detector images and converted to units rayleigh (R). The analysis is carried out in the native detector frame and original pixel resolution without smoothing or binning. Errors are calculated and propagated for each pixel in an image considering all statistical and systematic uncertainties of the HST pipeline (including bad pixels) and our processing steps (c.f. (Roth et al., 2016)). Figure 1 shows the two oxygen images (a and b) from visit 13 of the trailing hemisphere as an example with good signal-to-noise ratio. The emissions reveal the typical morphology that is determined by the interaction with the plasma environment (Roth et al., 2016).

Table 1. Parameters of the HST/STIS observations, first published in Roth et al. (2016). CML refers to the Central Meridian (West) Longitude on Europa's disk, Jupiter's planetocentric longitude facing Europa is given by the System-III longitude.

Visit	Observed Hemisphere	Date	Start time (UTC)	End time (UCT)	No. of exp.	Used (total) exp.time [min]	Europa diameter [arcsec]	Spatial resolution [km/pixel]	Europa CML [°]	System-III longitude [°]
17a	Eclipse	2015-03-23	23:14	23:41	1	26.9 (26.9)	0.92	83.0	10-12	146-161
17b	Egress	2015-03-24	00:27	01:12	1	30.3 (45.6)	0.92	83.0	16-18	194-209
1	Trailing	1999-10-05	08:39	15:32	5	142.2 (156.0)	1.07	71.5	245-274	300-161
2	Trail./Anti-J.	2012-11-08	20:41	03:33	5	155.0 (183.4)	1.04	73.9	209-238	24-244
3	Leading	2012-12-30	18:49	01:39	5	140.1 (164.1)	1.02	74.9	79-108	360-220
4	Lead./Anti-J.	2014-01-22	14:02	20:53	5	143.4 (183.4)	1.01	76.0	117-146	201- 61
13	Trailing	2015-02-22	11:00	16:17	4	154.6 (171.2)	0.98	78.3	256-278	132-301
14	Leading	2015-02-24	05:58	12:51	5	195.3 (217.0)	0.98	78.4	77-107	67-288
15	Trail./Sub-J.	2015-03-09	01:03	08:01	5	193.4 (232.0)	0.96	80.2	296-325	189- 52
16	Lead./Anti-J.	2015-03-21	16:59	22:21	4	145.0 (183.3)	0.93	82.4	141-163	209- 21

The focus of this study is on the oxygen emission *ratio*. To achieve reasonable signal-to-noise levels (c.f. the noisy ratio images in figure 2-4 of (Roth et al., 2016)), we calculate average ratios in larger regions and binned profiles across the images, by dividing the averaged intensity of the OI1356 Å by the averaged intensity of the OI1304 Å in *all pixels* within the respective bins or areas.

In Figure 2(b-d), we show the oxygen emission ratio averaged over three radial regions, as sketched in panel (a), for all analyzed image pairs. Panel (b) shows the ratio in the *limb* region, which includes all pixels centered at radial distances between 0.75 R_E

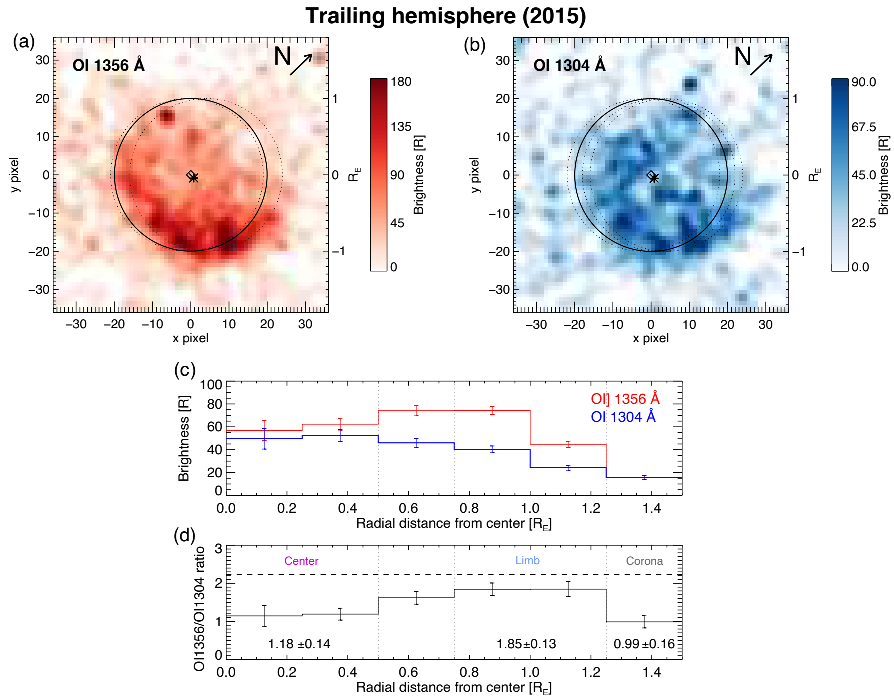

Figure 1. (a) and (b): HST/STIS images of the oxygen emission at OI 1356 Å (left) and OI 1304 Å (right) above Europa's trailing hemisphere observed during visit 13 on 2015-2-22. The images were smoothed twice with a 3x3 pixel boxcar function. All analysis was carried out with the original data, i.e., no binning or smoothing is applied.. The vectors marked 'N' show the direction to Jupiter North. The slightly dispersed locations of Europa's disk at the individual oxygen multiplet lines are shown by dotted circles. Diamonds indicate the disk center and the asterisks the sub-solar point. (c) Radial intensity profile for both oxygen emissions with angular bins of 0.25 R_E derived from the images. (d) Radial profile of the oxygen emission ratio, $r_\gamma(\mathrm{OI})$, derived from the observations in (c). The numbers indicate the derived ratios with uncertainties averaged over in the central, limb and coronal regions, respectively (dotted vertical lines, see also sketch in Figure 2a). The dashed line shows the ratio for a pure O_2 atmosphere.

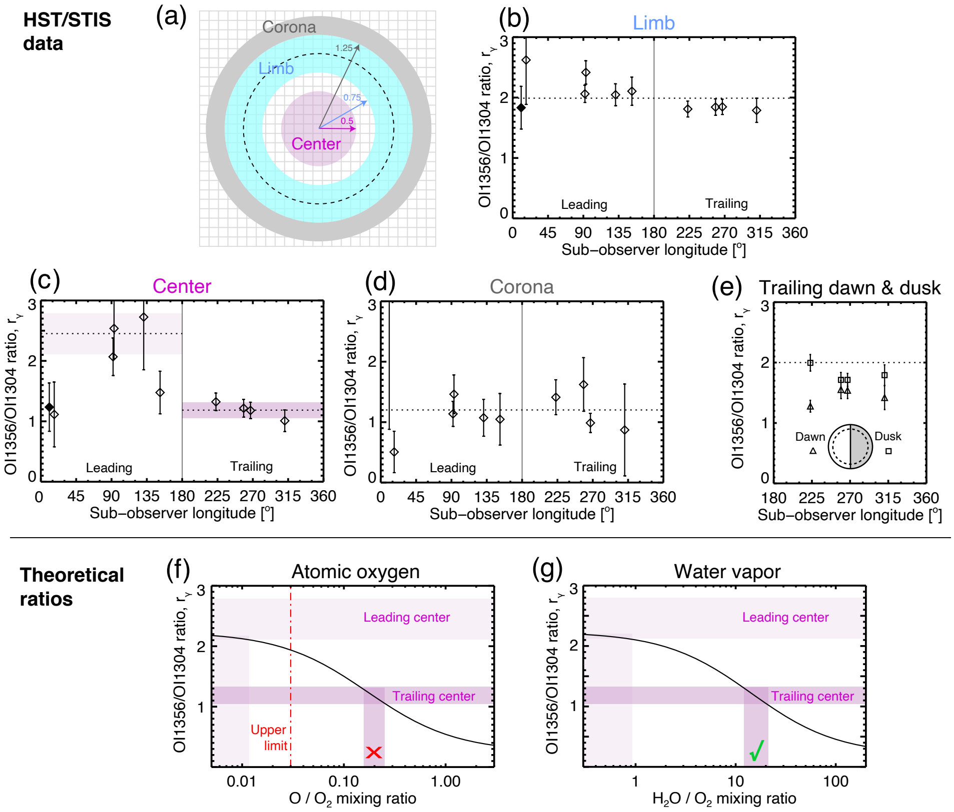

Figure 2. (a) Sketch of the three analyzed regions on and around Europa's disk, which is indicated by the dashed circle. If the center of a pixel falls within the defined radial ranges it is counted for the respective region. (b), (c) and (d) Oxygen emission ratios, r_γ(OI), for the three regions. The dashed lines in (b) and (c) show the mean of all visits (except the eclipse/egress exposures). In (d), the light purple shaded area shows variance range of the three images near 90° W longitude, the darker purple shaded area show the standard deviation range around the mean of all four images of the trailing side >180° W longitude. (e) Oxygen emission ratios, r_γ(OI), on the dawn side (triangles) and dusk (squares) side (all pixels within 1.25 R_E on either half of the circle, see sketch in inlet) for four the trailing hemisphere images. (f) and (g) Theoretical emission ratio as a function of the relative abundance of atomic oxygen, O, and water vapor, H_2O, in an O_2 atmosphere for electron impact excitation.

and 1.25 R_E from Europa's disk center. The ratios derived in the *center* region (<0.5 R_E) is shown in panel (c), and the ratio in a *coronal* region (1.25 R_E < r <1.5 R_E) is shown in panel (d).

3 Excitation Model

We consider electron impact excitation as well as resonant scattering of the solar OI1304 Å radiation, using the same emission rates from electron impact (dissociative) excitation of O_2, H_2O and O as in Roth et al. (2016, 2021) based on the cross sections from Doering and Gulcicek (1989), Kanik et al. (2001), Kanik et al. (2003), and Makarov et al. (2004). The focus of this study is on the OI1356 Å/OI1304 Å ratio, which is independent of the *density* of the exciting electrons and relatively insensitive to the electron temperature (if resonant scattering is neglected). The OI1356 Å/OI1304 Å ratio is yet sensitive to the atmospheric abundance of H_2O and O relative to O_2.

Following the previous studies, we assumed a thermal electron population with 20 eV plus a 5% higher temperature fraction at 250 eV and calculate an effective emission rate for this population. For the emission rate for OI1356 Å from dissociative excitation H_2O, we scaled the rate for OI1304 Å by a factor of 0.2 based on the laboratory measurements of Makarov et al. (2004) for 100 eV electrons. The resulting oxygen emission ratio from electron-impact excitation as a function of the O/O_2 and H_2O/O_2 abundance ratios in the atmosphere are shown in Figure 2f and g.

For the estimates of absolute neutral abundances, we assume an electron density of 160 cm^{-3} following de Kleer and Brown (2018). Although this is 4× higher than the density of 40 cm^{-3} assumed in some previous studies of Europa's far-UV emissions (Hall et al., 1995; Hall et al., 1998; Roth et al., 2016), it is in better agreement with the latest studies of the Europa plasma environment (Bagenal et al., 2015; Bagenal & Dols, 2020).

Resonant scattering of the solar OI1304 Å is calculated in the optically thin limit with a resonant scattering g factor of 5×10^{-7} 1/s (Cunningham et al., 2015). Hence, 1 R of OI1304 Å emission relates to an O column density of 2×10^{12} cm^{-2}.

4 Results and Interpretation

4.1 Eclipse test

The comparison of the eclipse exposure to the after-eclipse exposure suggests that resonant scattering by atomic oxygen is negligible. The image-averaged OI1304 Å and OI1356 Å intensities in eclipse are 21.9(±2.7) R and 40.2(±3.4) R, respectively. The intensities in the following exposure taken after egress were 15.8(±3.2) R and 36.3(±3.5) R, corresponding to a decrease by 28(±23)% for OI1304 Å and 10(±11)% for OI1356 Å. Thus, both emissions appear to be weaker after eclipse, suggesting a lower auroral excitation. This is consistent with the fact that Europa is moving away from the plasma sheet during this eclipse/egress visit (Table 1). The similar decrease at OI1304 Å compared to OI1356 Å indicates that resonant scattering of solar light, which would add to the OI1304 Å emission (only) and thus lead to an increase (or weaker decrease), is negligible.

Based on the change in OI1356 Å, we assume that 10(±11)% of the change in OI1304 Å is due to auroral excitation. After this correction for auroral changes, the residual OI1304 Å intensity change and the propagated related uncertainty are −3.9±3.5 R, thus consistent with no change apart from auroral effects within 1.1σ. Setting an upper limit for the change of +3 R (corresponding to $\sim 2\sigma$ of the measured change of −3.9±3.5 R) for the resonant scattering contribution at OI1304 Å over Europa's disk, we get an upper limit for the vertical O column density averaged of the same area of 6×10^{12} cm^{-2}.

Considering various aspects of the variable plasma environment and the atmospheric distribution, the minimum O_2 column density in Europa's atmosphere is estimated to be 2×10^{14} cm^{-2} (Hall et al., 1998; Roth et al., 2016; de Kleer & Brown, 2018). The upper limit for the O abundance derived above and this minimum O_2 abundance imply a maximum O/O_2 ratio in the atmosphere of 0.03 (red dash-dotted line in Figure 2f).

We note that the change observed in the coronal region (1.25 $R_E < r <$1.5 R_E) is different. While the OI1356 Å intensity again decreases, from 14.8(±3.9) R (eclipse) to 6.4(±4.0) R (sunlight), the OI1304 Å emission *increases* from 4.7(±3.2) R (eclipse) to 12.7(±4.0) R. This can also be seen in Figure 2d: the oxygen emission ratio in the corona drops from r_γ(OI) $\sim$ 3.1 in the eclipse exposure (off the vertical range) to r_γ(OI) $\sim$ 0.5 after egress (near sub-observer longitude 10°). The *increase* in OI1304 Å in the corona region is consistent with resonant scattering contributing to the overall faint signal, possibly originating from Europa's extended atomic corona (Hansen et al., 2005; Smith et al., 2019). However, the error ranges in these individual exposure are large and small systematic uncertainties in the background subtraction (not reflected in the error bar) might lead to additional uncertainties for the faint coronal emission. We also note that the OI1304 Å increase of 8.0($\pm$5.1) R in the corona region (neglecting possible changes due to changing auroral excitation) is also consistent (within the propagated uncertainty) with our 3 R upper limit for resonant scattering in the bound atmosphere derived above.

4.2 Oxygen emission ratio profiles in the images

Next, we investigate the oxygen emission ratios in the three regions across the disk: corona, limb, and central region. The comparison of the derived ratios for all images (Figure 2b-d) reveals some systematic differences, both between the regions as well as between the observed hemispheres.

In the *limb* region, the oxygen emission ratio is similar for all visits (i.e., independent of observing geometry) and consistent with their mean value of $\langle r_\gamma(\mathrm{OI})\rangle = 2.0$ (dotted line in Figure 2b) within the individual $\sim$1-σ uncertainties. There appears to be a marginal trend with somewhat lower ratios on the trailing and somewhat higher ratios on the leading side. These ratios are consistent with a predominantly O_2 atmosphere with a small O mixing ratio near the upper limit derived for the bound atmosphere of $O/O_2 = 0.03$ (Figure 2f).

In the *coronal* region, the ratios are systematically lower and again consistent within 1-σ with their mean of $\langle r_\gamma(\mathrm{OI})\rangle = 1.2$ (dotted line in Figure 2d) for almost all analyzed visits. These results agree well with our previous similar analysis of the coronal emission ratio in the same data, see table 2 and figure 9B in Roth et al. (2016). The low ratio can be explained by a higher O/O_2 abundance ratio in the corona than in the bound atmosphere (Roth et al., 2016). The upper limit on O/O_2 was derived within 1.25 R_E, i.e., for the bright emissions and the denser near-surface atmosphere, but it does not apply for the coronal region. The intensities of both oxygen emissions in the corona are only around 10 R, consistent with column densities of a few $\sim 10^{13}$ cm^{-2} for O_2 and a few $\sim 10^{12}$ cm^{-2} for O, and a relative abundance of $O/O_2 \sim 0.2$.

In the *center* region, there appears to be a systematic difference between the images and in particular between images of the trailing hemisphere and some of the images of the leading hemisphere (Figure 2c).

First, we look at the leading side images with sub-observer longitude of 90($\pm$45)°, i.e., where the leading meridian longitude (90°) is $\leq$45° offset from the central meridian longitude in the image. In the three images in this category, the center emission ratio is similar to (slightly higher than) the limb emission ratio with a mean of $\langle r_\gamma(\mathrm{OI})\rangle =$ 2.4 (dotted line in the 0°-180° range, Figure 2c). This high ratio is consistent with a pure O_2 atmosphere.

For the four trailing side images, the emission ratios in the center are consistently lower and well below 2 with a mean value of $\langle r_\gamma(\mathrm{OI})\rangle = 1.2$ (Figure 2c), similar to the corona region. In contrary to the corona, however, this can not be explained by a higher O/O_2 ratio. In the trailing center region, the intensities of both oxygen emissions are $\sim$50 R or higher (see example intensity profiles in Figure 1c) and the upper limit of O/O_2 derived above for the bound atmosphere applies. Since an O/O_2 ratio of $\sim$0.2 would be required to explain the the low r_γ(OI) (see Figure 2f), i.e., $\sim$10 times above the upper limit, atomic oxygen can be ruled out even when considering the possibility of O being concentrated to the central region.

The radial profiles of the oxygen emission ratio in smaller 0.25-R_E bins in the four trailing hemisphere images reveled a general and consistent behaviour, shown for an example visit from 2015 in Figure 1d. The emission ratio peaks near the limb, i.e., near radius $r = 1\mathrm{R_E}$. Away from the limb, the emission ratio systematically decreases both towards higher altitudes above the limb and towards the disk center. This is the same profile as observed for Ganymede (Roth et al., 2021).

We then consider electron-impact excitation of H_2O as the process cause the low oxygen emission ratio, r_γ(OI), in the central disk region. The derived value of $r_\gamma(\mathrm{OI}) = 1.2\pm0.2$ then is consistent with H_2O/O_2 ratios between 12 and 22 (see Figure 2g) and thus an H_2O-dominated atmosphere in the trailing center atmosphere.

Next we look at the visit, when Europa's anti-Jovian hemisphere was mostly observed (near sub-observer longitude 150°). The derived ratio of $r_\gamma(\mathrm{OI}) = 1.5 \pm 0.3$ is between the leading and trailing side values. We refrain from interpreting this value further, as there is an additional uncertainty due to the observing geometry. In this observation of the anti-Jovian side of Europa in its tidally locked orbit, the relatively small angular separation from Jupiter allows for possible nearby emissions from the Io torus, which introduce an extra uncertainty in the background subtraction. Because such torus background would be blocked by Europa, the determination of the background brightness away from the moon might lead to an over-subtraction of this background signal on the disk. This affects both the solar reflection (via the albedo) modelling and the emissions directly.

Finally, in the two individual exposures in eclipse and after egress (near sub-observer longitude 15°) the low ratios of $r_\gamma(\mathrm{OI}) = 1.2\pm0.4$ (eclipse) and $r_\gamma(\mathrm{OI}) = 1.1\pm0.5$ (after egress) are very similar to the trailing side ratio. Hence, these ratios are similarly consistent with a substantial H_2O abundance in the central region. This would imply that the H_2O atmosphere in the central disk region is present even on the sub-Jovian hemisphere and throughout the eclipse passage. However, the uncertainties prevent firm conclusions.

We searched for further trends in the emision ratio across the images. Directional profiles along the east-west and south-north directions generally resembled the radial profiles with higher r_γ(OI) near the limb. In some images, there appear to be trends, but these were not consistently seen in all images and seem to be transient and possibly even due to statistical fluctuations.

Figure 2e shows a systematic trend that is possibly present on the trailing hemisphere. Here the emission ratio r_γ(OI) averaged over the dawn half disk and the average ratio on the dusk half disk (all pixels within 1.25 $\mathrm{R_E}$ on either side) are compared. We found that r_γ(OI) is lower on the dawn half disk than on the dusk half disk in all four images of the trailing side (while no systematic behaviour was found in the leading side images). Interpretations of this possible trend will be further discussed in the final section.

4.3 Estimates of trailing hemisphere H_2O abundance.

We estimate absolute abundances for H_2O and O_2 on the trailing hemisphere from the OI1356 Å and OI1304 Å intensities using the values measured during visit 13 (Figure 1), where the emission intensities had an average level (see, e.g., figure 6 of Roth et al. (2016)). We assume a fixed O column density at the upper level derived above. Using the model assumptions for the exciting electron population and described in Section 3 and taking into account resonant scattering by O, we then simultaneously fit the O_2 and H_2O column densities to match the observed intensities of the two oxygen emissions.

The results from the fitting (Table 2) confirm not only that in the center region the abundance of H_2O is about an order of magnitude higher than that of O_2, but also

Table 2. Observed intensities during visit 13 and fitted column densities and the model emissions for the three considered species.

	Center region			Limb region		
Observation		*OI1356 Å*	*OI1304 Å*		*OI1356 Å*	*OI1304 Å*
STIS visit 13		61 ± 4 R	52 ± 5 R		58 ± 2 R	31 ± 2
Species	*Column density* (cm^{-2})	*OI1356 Å*	*OI1304 Å*	*Column density* (cm^{-2})	*OI1356 Å*	*OI1304 Å*
H_2O	2.95×10^{15}	4.6 R	20.6 R	$< 1 \times 10^{13}$	< 0.1 R	< 0.1 R
O_2	2.47×10^{14}	55.5 R	24.9 R	2.54×10^{14}	56.6 R	25.3 R
O	6×10^{12} *	0.9 R	6.5 R†	6×10^{12} *	0.9 R	6.5 R†
Total	–	61.0 R	52.0 R	–	57.5 R	31.8 R

* The O abundance is set to the derived upper limit
† The OI1304 intensity from O includes a resonant scattering contribution of 3 R.

that in the limb region H_2O is not required to explain the measurements. The limb intensities are well in agreement with a dominant O_2 atmosphere with low atomic oxygen abundance with $O/O_2 = 0.024$. If the global abundance of O is lower, a small amount of H_2O is required in the limb region and a slightly more H_2O is needed in the center.

We emphasize again that the total abundances are sensitive to the electron properties. We omitted to state uncertainty ranges for the fitted abundances in Table 2, which would only reflect the comparably small statistical uncertainties of about $\leq$10%. The uncertainty of the electron properties is, however, considerably larger than this. When assuming a homogeneous distribution of the electrons around Europa, the neutral densities scale inversely with the assumed electron density (see figure 12a in Roth et al. (2016)). For example, in the case of a two times lower electron density, twice higher neutral abundances are required. In reality the electrons will cool in the atmosphere due to collisions and the aurora yield will be sensitive to the details of this interaction (Saur et al., 1998; Rubin et al., 2015; Dols et al., 2016).

5 Discussion and Conclusions

The slightly updated treatment of the solar reflection signal modeling described change the results only marginally compared to our previous study on the same data and we found that all numbers are consistent within uncertainties with the results of Roth et al. (2016).

The upper limit of the atomic to molecular oxygen ratio of $O/O_2 = 0.03$ is similar to the O mixing ratio derived for Europa from Cassini UVIS measurements of 0.02 (Hansen et al., 2005) and to the upper limit of 0.02 for Ganymede found in an HST eclipse test (Roth et al., 2021).

The oxygen emission ratio is systematically and significantly below the value for a pure O_2 atmosphere in the central trailing hemisphere. Based on the derived upper limit, resonant scattering and electron excitation of O can not cause the low oxygen emission ratio in this region. Electron impact dissociative excitation of H_2O is the most likely viable process to produce the reduced ratio. In addition, two different species are a logical explanation for the particular shape of the radial profiles with a peak ratio near the limb (close to pure O_2) and two separate minima above the limb (due to O) and in the disk center (due to H_2O). Contributions from other possible species like OH or CO_2 are negligible due to the low expected abundances and low emission cross sections (McGrath et al., 2004; McConkey et al., 2008).

The abundance of H_2O relative to O_2 derived for Europa's trailing hemisphere of H_2O/O_2 = 12–22 is similar to the values found for Ganymede's trailing hemisphere (H_2O/O_2

= 12-32). On Europa's leading hemisphere, there is no indication for the presence of H_2O, as the oxygen emission ratios are even higher in the center region than near the limb.

Our estimate for the absolute H_2O abundance of 3×10^{15} cm^{-2} can be compared to the Keck search for infrared H_2O emissions (Paganini et al., 2019) and in particular to their most sensitive measurement of the same hemisphere (February 27 in table 2 of Paganini et al. (2019)). Their slit-average column density upper limit of 1.3×10^{15} cm^{-2} is 2.3 times lower than our estimated value. However, the slit covers an area of about 3250 km $\times$ 1500 km and hence large areas across Europa's disk and slightly outside the disk. Because the H_2O abundance apparently rapidly decreases to negligible abundances outside the central area, i.e., between radii $r = 0.5$ R_E and $r = 0.75$ R_E, the disk-average (or slit-average for the Keck data) column density is expected to be lower by a factor of about 2-4 than the density derived here for the disk center only. Hence, our values are consistent with the Keck upper limit.

A key finding of this study is the consistency in the detection of the reduced oxygen emission ratio on the trailing hemisphere disk center and the overall stability of the ratio profiles in all images with similar geometry. In particular, the oxygen emission ratios in center and limbs regions in the four trailing side visits, which were obtained in 1999, 2012, and 2015 and are all consistent within uncertainties. This means, they are diagnostic for persistent atmospheric properties, in stark contrast to the apparent transient nature of detected features that were interpreted to relate to H_2O plumes (Roth, Saur, Retherford, Strobel, et al., 2014; Paganini et al., 2019).

Persistent sources for H_2O can be sublimation or sputtering by charged particles of the surface ices, which both can produce a hemispheric difference between the leading and trailing day side hemispheres.

The sublimation yield is sensitive to temperature and the ice fraction of the surface material. Both measurements (Spencer et al., 1999; Rathbun et al., 2010; Trumbo et al., 2018) and modeling (Oza et al., 2019) of the surface properties suggest higher temperatures on the visibly darker (McEwen, 1986) trailing hemisphere, possibly leading to higher sublimated H_2O abundance there.

The trailing hemisphere also coincides with the plasma upstream hemisphere, where most of the thermal plasma impinges on Europa's surface according to modelling (Pospieszalska & Johnson, 1989; Cassidy et al., 2013). In addition, the sputtering yield (amount of neutrals ejected per incident charged particle flux) also increases with surface temperature (Famá et al., 2008), further favoring the trailing hemisphere independent of the distribution of the incident flux.

For both sources, however, modelled H_2O abundances are often significantly lower than our derived value on the trailing side (Shematovich et al., 2005; Smyth & Marconi, 2006; Plainaki et al., 2013). The H_2O sublimation flux at Europa's maximum surface temperatures of 130 K is about two orders of magnitude lower (Feistel & Wagner, 2007) than for Ganymede's surface temperature of 145 K (Orton et al., 1996). H_2O yield from sputtering similarly is estimated to be too low to sustain column densities larger than $\sim 10^{13}$ cm^{-2} for the short-lived H_2O molecues, which freeze and are lost from the atmosphere upon surface contact (Shematovich et al., 2005; Smyth & Marconi, 2006; Plainaki et al., 2013).

The atmosphere modelling study of Teolis et al. (2017) considers secondary sublimation, i.e., sublimation of sputtered H_2O molecules that fall back to the surface, as source in addition to sputtering. In their results the H_2O abundance exceeds the O_2 abundance on the dayside, with column densities up to 1.3×10^{15} cm^{-2} (their tables 2 and 3). Thus, according to the results of Teolis et al. (2017), the combined effects of sputtering and sublimation of fresh H_2O deposits might be the source for the detected H_2O atmosphere.

The lower r_γ(OI) on the dawn side compared to the dusk side of the trailing hemisphere (Figure 2e) can be explained by a relatively stronger emission contribution from H_2O or higher H_2O/O_2 abundance ratio in the dawn sector (or lower H_2O/O_2 ratio in dusk sector). O can be ruled out as main cause for the differing oxygen emission ratios with the same arguments as above. This difference in H_2O/O_2 abundance ratios between dawn and dusk is conistent with the surplus of O_2 on the dusk side suggested by a modelling study (Oza et al., 2019). Roth et al. (2016) showed that the absolute OI1356 Å intensities are also systematically higher on the dusk side in nearly all images. The vast majority of the OI1356 Å emissions originate from O_2 (due to the ~160 higher emission OI1356 Å rate from O_2 compared to H_2O) and are thus insensitive to the abundance of H_2O. Therefore, a surplus of O_2 on the dusk side compared to the dawn side (and assuming the H_2O abundance is symmetric) is a consistent explanation for the dawn-dusk asymmetries both in the absolute OI1356 Å intensity found in Roth et al. (2016) and in the dawn and dusk emission ratios derived here.

Putting the main results in a nutshell, oxygen emission ratios found in HST observations suggest a persistent H_2O atmosphere above Europa's trailing hemisphere, but the source of the water vapor can not unambigously identified.

Acknowledgments

The HST data used in this work were taken within programs HST-GO-8224, HST-GO-13040, HST-GO-13619, HST-GO-13679, and are available on the MAST archive of STScI at https://archive.stsci.edu/proposal_search.php?mission=hst&id=8224, https://archive.stsci.edu/proposal_search.php?mission=hst&id=13040, https://archive.stsci.edu/proposal_search.php?mission=hst&id=13619, and https://archive.stsci.edu/proposal_search.php?mission=hst&id=13679.

References

Bagenal, F., & Dols, V. (2020, May). The Space Environment of Io and Europa. *Journal of Geophysical Research (Space Physics)*, *125*(5), e27485. doi: 10.1029/2019JA027485

Bagenal, F., Sidrow, E., Wilson, R. J., Cassidy, T. A., Dols, V., Crary, F. J., ... Paterson, W. R. (2015, November). Plasma conditions at Europa's orbit. *Icarus*, *261*, 1-13. doi: 10.1016/j.icarus.2015.07.036

Cassidy, T. A., Paranicas, C. P., Shirley, J. H., Dalton, J. B., III, Teolis, B. D., Johnson, R. E., ... Hendrix, A. R. (2013, March). Magnetospheric ion sputtering and water ice grain size at Europa. *Planetary and Space Science*, *77*, 64-73. doi: 10.1016/j.pss.2012.07.008

Cunningham, N. J., Spencer, J. R., Feldman, P. D., Strobel, D. F., France, K., & Osterman, S. N. (2015). Detection of callisto's oxygen atmosphere with the hubble space telescope. *Icarus*, *254*, 178–189.

de Kleer, K., & Brown, M. E. (2018, Oct). Europa's Optical Aurora. *AJ*, *156*(4), 167. doi: 10.3847/1538-3881/aadae8

Doering, J. P., & Gulcicek, E. E. (1989, February). Absolute differential and integral electron excitation cross sections for atomic oxygen. VII - The ^{3}P-^{1}D and ^{3}P-^{1}S transitions from 4.0 to 30 eV. *J. Geophys. Res.*, *94*, 1541–1546. doi: 10.1029/JA094iA02p01541

Dols, V. J., Bagenal, F., Cassidy, T. A., Crary, F. J., & Delamere, P. A. (2016, January). Europa's atmospheric neutral escape: Importance of symmetrical O_2 charge exchange. *Icarus*, *264*, 387-397. doi: 10.1016/j.icarus.2015.09.026

Famá, M., Shi, J., & Baragiola, R. A. (2008). Sputtering of ice by low-energy ions. *Surface Science*, *602*, 156-161. doi: 10.1016/j.susc.2007.10.002

Feistel, R., & Wagner, W. (2007, January). Sublimation pressure and sublimation enthalpy of H $_2$O ice Ih between 0 and 273.16 K. *Geochim. Cosmochim. Acta*, *71*(1), 36-45. doi: 10.1016/j.gca.2006.08.034

Feldman, P. D., A'Hearn, M. F., Bertaux, J.-L., Feaga, L. M., Parker, J. W., Schindhelm, E., … Vincent, J.-B. (2015, November). Measurements of the near-nucleus coma of comet 67P/Churyumov-Gerasimenko with the Alice far-ultraviolet spectrograph on Rosetta. *A&A*, *583*, A8. doi: 10.1051/0004-6361/201525925

Feldman, P. D., McGrath, M. A., Strobel, D. F., Moos, H. W., Retherford, K. D., & Wolven, B. C. (2000, June). HST/STIS Ultraviolet Imaging of Polar Aurora on Ganymede. *Astrophys. J.*, *535*, 1085–1090. doi: 10.1086/308889

Galand, M., Feldman, P. D., Bockelée-Morvan, D., Biver, N., Cheng, Y. C., Rinaldi, G., … Burch, J. (2020, September). Far-ultraviolet aurora identified at comet 67P/Churyumov-Gerasimenko. *Nature Astronomy*, *4*, 1084-1091. doi: 10.1038/s41550-020-1171-7

Giono, G., Roth, L., Ivchenko, N., Saur, J., Retherford, K., Schlegel, S., … Strobel, D. (2020, April). An Analysis of the Statistics and Systematics of Limb Anomaly Detections in HST/STIS Transit Images of Europa. *AJ*, *159*(4), 155. doi: 10.3847/1538-3881/ab7454

Hall, D. T., Feldman, P. D., McGrath, M. A., & Strobel, D. F. (1998, May). The far-ultraviolet oxygen airglow of Europa and Ganymede. *Astrophys. J.*, *499*(5), 475–481.

Hall, D. T., Strobel, D. F., Feldman, P. D., McGrath, M. A., & Weaver, H. A. (1995, February). Detection of an oxygen atmosphere on Jupiter's moon Europa. *Nature*, *373*(6516), 677–679.

Hansen, C. J., Shemansky, D. E., & Hendrix, A. R. (2005). Cassini UVIS observations of Europa's oxygen atmosphere and torus. *Icarus*, *176*(2), 305–315.

Johnson, R. E., Burger, M. H., Cassidy, T. A., Leblanc, F., Marconi, M., & Smyth, W. H. (2009). Composition and Detection of Europa's Sputter-induced Atmosphere. In R. T. Pappalardo, W. B. McKinnon, & K. K. Khurana (Eds.), *Europa* (p. 507). University of Arizona Press.

Kanik, I., Johnson, P. V., Das, M. B., Khakoo, M. A., & Tayal, S. S. (2001, July). Electron-impact studies of atomic oxygen: I. Differential and integral cross sections; experiment and theory. *Journal of Physics B: Atomic, Molecular and Optical Physics*, *34*, 2647-2665.

Kanik, I., Noren, C., Makarov, O. P., Vatti Palle, P., Ajello, J. M., & Shemansky, D. E. (2003, November). Electron impact dissociative excitation of O_2: 2. Absolute emission cross sections of the OI(130.4 nm) and OI(135.6 nm) lines. *J. Geophys. Res.*, *108*, 5126. doi: 10.1029/2000JE001423

Leblanc, F., Oza, A. V., Leclercq, L., Schmidt, C., Cassidy, T., Modolo, R., … Johnson, R. E. (2017, September). On the orbital variability of Ganymede's atmosphere. *Icarus*, *293*, 185-198. doi: 10.1016/j.icarus.2017.04.025

Makarov, O. P., Ajello, J. M., Vatti Palle, P., Kanik, I., Festou, M. C., & Bhardwaj, A. (2004, September). Kinetic energy distributions and line profile measurements of dissociation products of water upon electron impact. *J. Geophys. Res.*, *109*(A18), 9303.

McConkey, J. W., Malone, C. P., Johnson, P. V., Winstead, C., McKoy, V., & Kanik, I. (2008, September). Electron impact dissociation of oxygen-containing molecules A critical review. *Phys. Rep.*, *466*(1-3), 1-103. doi: 10.1016/j.physrep.2008.05.001

McEwen, A. S. (1986, July). Exogenic and endogenic albedo and color patterns on Europa. *J. Geophys. Res.*, *91*, 8077-8097. doi: 10.1029/JB091iB08p08077

McGrath, M. A., Hansen, C. J., & Hendrix, A. R. (2009). Observations of Europa's Tenuous Atmosphere. In R. T. Pappalardo, W. B. McKinnon, & K. K. Khurana (Eds.), *Europa* (p. 485-505). University of Arizona Press.

McGrath, M. A., Lellouch, E., Strobel, D. F., Feldman, P. D., & Johnson, R. E. (2004). Satellite atmospheres. In Bagenal, F., Dowling, T. E., & McKinnon,

W. B. (Ed.), *Jupiter. the planet, satellites and magnetosphere* (pp. 457–483). Cambridge University Press.

Molyneux, P. M., Nichols, J. D., Bannister, N. P., Bunce, E. J., Clarke, J. T., Cowley, S. W. H., ... Paty, C. (2018, May). Hubble Space Telescope Observations of Variations in Ganymede's Oxygen Atmosphere and Aurora. *Journal of Geophysical Research (Space Physics)*, *123*(5), 3777-3793. doi: 10.1029/2018JA025243

Oren, M., & Nayar, S. K. (1994). Generalization of lambert's reflectance model. In *Proceedings of the 21st annual conference on computer graphics and interactive techniques* (pp. 239–246).

Orton, G. S., Spencer, J. R., Travis, L. D., Martin, T. Z., & Tamppari, L. K. (1996, October). Galileo Photopolarimeter-Radiometer Observations of Jupiter and the Galilean Satellites. *Science*, *274*, 389-391. doi: 10.1126/science.274.5286.389

Oza, A. V., Leblanc, F., Johnson, R. E., Schmidt, C., Leclercq, L., Cassidy, T. A., & Chaufray, J.-Y. (2019, March). Dusk over dawn O_2 asymmetry in Europa's near-surface atmosphere. *Planet. Space Sci.*, *167*, 23-32. doi: 10.1016/j.pss.2019.01.006

Paganini, L., Villanueva, G. L., Roth, L., Mand ell, A. M., Hurford, T. A., Retherford, K. D., & Mumma, M. J. (2019, Nov). A measurement of water vapour amid a largely quiescent environment on Europa. *Nature Astronomy*, 489. doi: 10.1038/s41550-019-0933-6

Plainaki, C., Milillo, A., Mura, A., Saur, J., Orsini, S., & Massetti, S. (2013, November). Exospheric O_2 densities at Europa during different orbital phases. *Planetary and Space Science*, *88*, 42-52. doi: 10.1016/j.pss.2013.08.011

Pospieszalska, M. K., & Johnson, R. E. (1989). Magnetospheric ion bombardment profiles of satellites: Europa and Dione. *Icarus*, *78*, 1–13.

Rathbun, J. A., Rodriguez, N. J., & Spencer, J. R. (2010, December). Galileo PPR observations of Europa: Hotspot detection limits and surface thermal properties. *Icarus*, *210*, 763-769. doi: 10.1016/j.icarus.2010.07.017

Roth, L., Ivchenko, N., Gladstone, G. R., Saur, J., Grodent, D., Bonfond, B., ... Retherford, K. D. (2021, July). A sublimated water atmosphere on Ganymede detected from Hubble Space Telescope observations. *Nature Astronomy*. doi: 10.1038/s41550-021-01426-9

Roth, L., Retherford, K. D., Saur, J., Strobel, D. F., Feldman, P. D., McGrath, M. A., & Nimmo, F. (2014, December). Orbital apocenter is not a sufficient condition for HST/STIS detection of Europa's water vapor aurora. *Proceedings of the National Academy of Science*, *111*, E5123-E5132. doi: 10.1073/pnas.1416671111

Roth, L., Saur, J., Retherford, K. D., Feldman, P. D., & Strobel, D. F. (2014, January). A phenomenological model of Io's UV aurora based on HST/STIS observations. *Icarus*, *228*, 386-406. doi: 10.1016/j.icarus.2013.10.009

Roth, L., Saur, J., Retherford, K. D., Strobel, D. F., Feldman, P. D., McGrath, M. A., & Nimmo, F. (2014, January). Transient Water Vapor at Europa's South Pole. *Science*, *343*, 171-174. doi: 10.1126/science.1247051

Roth, L., Saur, J., Retherford, K. D., Strobel, D. F., Feldman, P. D., McGrath, M. A., ... Ivchenko, N. (2016, March). Europa's far ultraviolet oxygen aurora from a comprehensive set of HST observations. *Journal of Geophysical Research (Space Physics)*, *121*, 2143-2170. doi: 10.1002/2015JA022073

Rubin, M., Jia, X., Altwegg, K., Combi, M. R., Daldorff, L. K. S., Gombosi, T. I., ... Wurz, P. (2015, May). Self-consistent multifluid MHD simulations of Europa's exospheric interaction with Jupiter's magnetosphere. *Journal of Geophysical Research (Space Physics)*, *120*, 3503-3524. doi: 10.1002/2015JA021149

Saur, J., Strobel, D. F., & Neubauer, F. M. (1998, August). Interaction of the

Jovian magnetosphere with Europa: Constraints on the neutral atmosphere. *J. Geophys. Res.*, *103*(E9), 19947–19962.

Shematovich, V. I., Johnson, R. E., Cooper, J. F., & Wong, M. C. (2005, February). Surface-bounded atmosphere of Europa. *Icarus*, *173*, 480-498. doi: 10.1016/j.icarus.2004.08.013

Smith, H. T., Mitchell, D. G., Johnson, R. E., Mauk, B. H., & Smith, J. E. (2019, January). Europa Neutral Torus Confirmation and Characterization Based on Observations and Modeling. *ApJ*, *871*(1), 69. doi: 10.3847/1538-4357/aaed38

Smyth, W. H., & Marconi, M. L. (2006, April). Europa's atmosphere, gas tori, and magnetospheric implications. *Icarus*, *181*, 510-526. doi: 10.1016/j.icarus.2005.10.019

Sparks, W. B., Hand, K., McGrath, M., Bergeron, E., Cracraft, M., & Deustua, S. E. (2016, December). Probing for evidence of plumes on Europa with HST/STIS. *ApJ*.

Spencer, J. R., Tamppari, L. K., Martin, T. Z., & Travis, L. D. (1999, May). Temperatures on Europa from Galileo Photopolarimeter-Radiometer: Nighttime Thermal Anomalies. *Science*, *284*, 1514. doi: 10.1126/science.284.5419.1514

Teolis, B. D., Wyrick, D. Y., Bouquet, A., Magee, B. A., & Waite, J. H. (2017, March). Plume and surface feature structure and compositional effects on Europa's global exosphere: Preliminary Europa mission predictions. *Icarus*, *284*, 18-29. doi: 10.1016/j.icarus.2016.10.027

Trumbo, S. K., Brown, M. E., & Butler, B. J. (2018, October). ALMA Thermal Observations of Europa. *AJ*, *156*(4), 161. doi: 10.3847/1538-3881/aada87